


Article

Surface Freshwater Fluxes in the Arctic and Subarctic Seas during Contrasting Years of High and Low Summer Sea Ice Extent

Sarah B. Hall ^{1,*}, Bulusu Subrahmanyam ¹ , Ebenezer S. Nyadjro ² and Annette Samuelsen ³

¹ School of the Earth, Ocean and Environment, University of South Carolina, Columbia, SC 29208, USA; sbulusu@geol.sc.edu

² Northern Gulf Institute, Mississippi State University, Stennis Space Center, MS 39529, USA; ebenezer@ngi.msstate.edu

³ Nansen Environmental and Remote Sensing Center, and Bjerknes Centre for Climate Research, N-5006 Bergen, Norway; annette.samuelsen@nersc.no

* Correspondence: shall@seoe.sc.edu

Abstract: Freshwater (FW) flux between the Arctic Ocean and adjacent waterways, predominantly driven by wind and oceanic currents, influences halocline stability and annual sea ice variability which further impacts global circulation and climate. The Arctic recently experienced anomalous years of high and low sea ice extent in the summers of 2013/2014 and 2012/2016, respectively. Here we investigate the interannual variability of oceanic surface FW flux in relation to spatial and temporal variability in sea ice concentration (SIC), sea surface salinity (SSS), and sea surface temperature (SST), focusing on years with summer sea-ice extremes. Our analysis between 2010–2018 illustrate high parameter variability, especially within the Laptev, Kara, and Barents seas, as well as an overall decreasing trend of FW flux through the Fram Strait. We find that in 2012, a maximum average FW flux of $0.32 \times 10^3 \text{ ms}^{-1}$ in October passed over a large portion of the Northeast Atlantic Ocean at 53°N . This study highlights recent changes in the Arctic and Subarctic Seas and the importance of continued monitoring of key variables through remote sensing to understand the dynamics behind these ongoing changes. Observations of FW fluxes through major Arctic routes will be increasingly important as the polar regions become more susceptible to warming, with major impacts on global climate.

Keywords: arctic; subarctic seas; freshwater flux; sea ice concentration; sea surface salinity; sea surface temperature; SMOS; SMAP



Citation: Hall, S.B.; Subrahmanyam, B.; Nyadjro, E.S.; Samuelsen, A. Surface Freshwater Fluxes in the Arctic and Subarctic Seas during Contrasting Years of High and Low Summer Sea Ice Extent. *Remote Sens.* **2021**, *13*, 1570. <https://doi.org/10.3390/rs13081570>

Academic Editors: Yi Luo and Viviane V. Menezes

Received: 5 March 2021

Accepted: 15 April 2021

Published: 18 April 2021

Publisher's Note: MDPI stays neutral with regard to jurisdictional claims in published maps and institutional affiliations.



Copyright: © 2021 by the authors. Licensee MDPI, Basel, Switzerland. This article is an open access article distributed under the terms and conditions of the Creative Commons Attribution (CC BY) license (<https://creativecommons.org/licenses/by/4.0/>).

1. Introduction

The Arctic Ocean serves as a dynamic link between the colder, fresher Pacific Ocean and the warmer, more saline Atlantic Ocean [1]. Despite covering only 3% of the Earth's total surface area, the Arctic and its subpolar regions play a crucial role in the regulation of meridional heat transport through thermohaline circulation [2,3]. The Arctic has increasingly sustained warming at a rate that is at least twice the global average due to the accumulation of anthropogenic stressors including increased greenhouse gas emissions within the atmosphere in recent decades [4]. This phenomenon, referred to as Arctic amplification, has a major long-term influence on the Arctic's cryosphere and hydrosphere, including the decline of annual sea ice extent (SIE) and freshwater (FW) storage in the Arctic and its fluidity to adjacent subpolar seas and oceans. These interactions propagate further into the lower latitudes, consequently influencing the global circulation and climate.

Overtaking caused by Arctic water deep convection is important for ocean ventilation. A slight increase in Arctic FW can contribute to stronger stratification, prohibiting advection and thus the regulation of global temperatures [5]. Rabe et al. [6] found an overall increase of $600 \pm 300 \text{ km}^3/\text{year}$ FW trend for the two decades leading up to 2012. On average, one

third of the Arctic FW input comes through the Bering Strait from the Pacific Ocean [7]. In contrast, the North Atlantic Ocean exchanges its warmer, more saline waters through the Norwegian and Barents Seas, for the Arctic's fresher waters that export through the Fram and Davis Straits [8,9]. The Arctic's FW budget is also regulated by river discharge, sea ice melt, and net precipitation; values which have been rising in conjunction with Arctic sea surface temperature (SST) and atmospheric wind stress [10]. McClelland et al. [11] accounted FW river exports to the Arctic to be over 10% of the global discharge, which Brown et al. [12] equates the largest source near Siberia at roughly $4.2 \times 10^3 \text{ km}^3/\text{year}$ and precipitation at $2.2 \times 10^3 \text{ km}^3/\text{year}$ during the first part of the 21st century. River runoff and net precipitation content can increase sea ice thickness as discussed by Weatherly et al. [13]. In this paper, we focus on the FW flux from marginal oceans and seas into and out of the Arctic ocean in relation to sea ice concentration (SIC). SIC refers to the amount of sea ice covering a specified area relative to the total area, given as a percentage in this study.

SIC growth (retreat) decreases (increases) the Arctic's FW content, making FW flux a good indicator for observing the distribution and intensity of Arctic sea ice on a regional and annual scale [14,15]. SIE, typically referenced as areas with a SIC above a 15% threshold, has declined at a rate of 4.7% per decade over the past four decades [16] with more recent rates of about 10–13% per decade [17,18]. Although commonly used, this threshold does have limitations when describing annual thinning of sea ice or depletion of multiyear sea ice [19]. Sea ice decline in the Arctic is regionally and temporally disproportionate, with a greater annual decrease shown within the Kara and Barents Seas compared to other arctic seas [20], and years experiencing abnormally low (2012 and 2016) and relatively high (2013 and 2014) minimum summer SIE in the past decade. The lowest summer SIE occurred in 2012 and covered 3.41 million km^2 [21,22]. A 48% increase in the following year of 2013 equated to roughly 5.35 million km^2 [23]. The lowest winter SIE occurred in March of 2016 which contributed to its low sea ice coverage of 4.14 million km^2 in the summer [24]. The alarming minimum SIE in 2012 followed by two consecutive high summer SIEs and then another low raised further concerns for the lack of predictability in Arctic sea ice trends; therefore, we observe significant variations of related, climatic parameters between these four years and within the past decade to better understand past causes, current trajectories, and future implications.

SST and sea surface salinity (SSS) influence SIC. The combination of solar radiation with atmospheric-to-ocean heat flux drives the strong seasonality of SST, influencing the conditions for sea ice to form or melt [25]. Higher SST limits the capacity of multi-year sea ice to form in the Arctic; an important feature describing the preservation of sea ice throughout the summer [26]. Sea ice formation (melt) causes local salinity to increase (decrease). SSS is also a reliable proxy for measuring the Arctic's FW flux between sources and exports [27]. Declining sea ice provides positive feedback by decreasing albedo and allowing more upward surface heat flux and increased SST that will continue to lessen ice accumulation [28]. SST is regionally important for sea ice patterns but tends to be generally uniform at near-freezing temperatures over the Arctic, making SSS and FW transport the main parameters that govern the convection and overturning dynamics of surface water masses to the deep ocean [5]. The lack of SIC allows for the fresher surface waters to endure oceanic stress between the atmospheric and surface water boundary [29,30]. Davis et al. [31] showed that even with a net increase of FW, the Arctic's halocline instability and vertical mixing are still determined by wind-driven motion on ice free ocean surfaces, which drive currents and could weaken the SIC in the Arctic. The direction and magnitude of wind and oceanic currents control FW variability through anticyclonic (cyclonic) tendencies that cause converging (diverging) interactions, leading to a build-up (release) of FW [32–34]. Ice drift speed increase poses a threat to perennial ice, leaving an Arctic dominated by the more vulnerable seasonal ice [35]. As Arctic conditions continue to change and the decline of annual sea ice becomes more apparent, winds will continually hinder the stability of sea ice formation and oceanic drifts will intensify [36].

The paucity of in-situ data within the Arctic is due to limited accessibility in its harsh environmental conditions. Satellite passive-microwave measurements within the Arctic and subarctic regions since 1979 have helped mitigate these uncertainties [37]. Although satellite data has bias, specifically with temperature sensitivity of L-band radiometry, research has shown its data to be accurate in communicating general Arctic trends and thus is a key component to observe the spatial and temporal scales where in-situ data are lacking [38]. In this study we use satellite-derived salinity from the European Space Agency's (ESA) Soil Moisture and Ocean Salinity (SMOS) and the National Aeronautics and Space Administration's (NASA) Soil Moisture Active Passive (SMAP) missions, for their spatial resolution and available timeframes [39,40]. SMAP retrieves 2- to 3-day temporal repetitions with 40 km spatial resolutions compared to the 3-day and 45–50 km temporal and spatial resolutions from SMOS [41]. For areas that both in-situ instruments and satellites cannot reach, i.e., sea surface areas covered by ice, ocean models provide an approximation of regional indices.

The main objective for this study is to analyze the influence of the polar region's FW flux impacted by related parameters during anomalous summer low (2012/2016) and relatively high (2013/2014) minimum SIEs. This study builds from the need to further understand FW flux processes affected by atmospheric and oceanic interrelations [15,18]. FW flux within the northern latitudes is important for the generation of the Arctic's strong stratification, marine biological production [42], mid-latitude weather patterns, and global circulation and climate [14,43]. Properties of SST, SSS, wind, and oceanic currents have been shown to fundamentally influence the annual variations of sea ice within the Arctic [44]. We divide the Arctic into three regions oriented around areas influenced by the Pacific Ocean, Atlantic Ocean, and the Canadian Arctic Archipelago (CAA). Results from this paper will help better understand the driving forces for and consequences of Arctic sea ice declination or growth; with supplementary influences on local wildlife, regional maritime advancements, oceanic circulation, and global climate change. The rest of this paper is ordered as follows: Section 2 describes data and methods, Section 3 illustrates research results, Section 4 deliberates discussion, and Section 5 summarizes conclusions of our study.

2. Materials and Methods

2.1. Data

We use the Group for High Resolution Sea Surface Temperature (GHR SST) Level-4 Canadian Meteorological Center (CMC) SST product [45]. This $0.2^\circ \times 0.2^\circ$ gridded product combines data from a variety of satellite sensors including the National Oceanic and Atmospheric Administration's (NOAA) Advanced Very High-Resolution Radiometer (AVHRR) and ESA's Along Track Scanning Radiometer (ATSR) series from ERS-1, ERS-2, and Envisat, as well as in-situ observations and buoys. SIC data for this study is produced as part of the U.K. Meteorological Office (UKMO) Operational Sea Surface Temperature and Sea Ice Analysis (OSTIA) product [46]. The $0.05^\circ \times 0.05^\circ$ gridded OSTIA ice concentration data is sourced from the EUMETSAT Ocean and Sea Ice Satellite Application Facility (OSI-SAF).

SMOS version 5 data for this study was obtained from L'OCEAN Centre Aval de Traitement des Données SMOS (CATDS) as a Level-3 monthly $0.25^\circ \times 0.25^\circ$ gridded product [47]. We also use SMAP Level-3 SSS Combined Active Passive (CAP) V5.0 data obtained from NASA's Jet Propulsion Laboratory (JPL) via the Physical Oceanography Distributed Active Archive Center (PO.DAAC) [48]. This $0.25^\circ \times 0.25^\circ$ gridded product is based on the newly released SMAP V5 Level-1 Brightness Temperatures. It uses an enhanced calibration methodology which improves absolute radiometric calibration and reduces the biases between ascending and descending passes. The SMOS mission has provided satellite SSS data since 2009 while the more recent launch of SMAP supplies data since mid-2015 [39,40].

Surface wind data for this study are from Remote Sensing Systems' (RSS) Cross-Calibrated Multi-Platform (CCMP) version 2.0, 6-hourly ocean vector wind analysis prod-

uct on a $0.25^\circ \times 0.25^\circ$ grid [49]. The CCMP dataset is produced by combining cross-calibrated satellite microwave winds and instrument observations using a Variational Analysis Method (VAM).

Due to limited coverage of satellite-derived ocean currents data in the Arctic, we use the Ocean Reanalysis System 5 (ORAS5) ocean current data from the European Centre for Medium-Range Weather Forecasts (ECMWF) [50]. ORAS5 has 75 vertically stratified layers and uses the Nucleus for European Modeling of the Ocean (NEMOv3.4) for its ocean model with a coupled sea ice model, and ERA-Interim and WAVE forcing with observational data assimilation. ORAS5 is available on a $0.25^\circ \times 0.25^\circ$ horizontal grid and is obtained from Integrated Climate Data Center (ICDC) at the University of Hamburg (<http://icdc.cen.uni-hamburg.de/projekte/easy-init/easy-init-ocean.html> accessed on: 29 January 2021).

2.2. Methods

2.2.1. Arctic Sectors for Time Series Analysis

We compute monthly mean fields from daily mean fields. In addition, we compute interannual anomalies by subtracting the monthly climatologies from the monthly time series. We then define low (2012 and 2016) and high (2013 and 2014) sea ice years based on the ice index from Fetterer et al. [51]. In order to analyze regional variations, we divide the Arctic Ocean into the following sectors (Figure 1):

Atlantic sector: 90°E – 45°W and 65°N – 90°N .

Canadian sector: 45°W – 40°W and 65°N – 90°N .

Pacific sector: 140°W – 90°E and 65°N – 90°N .

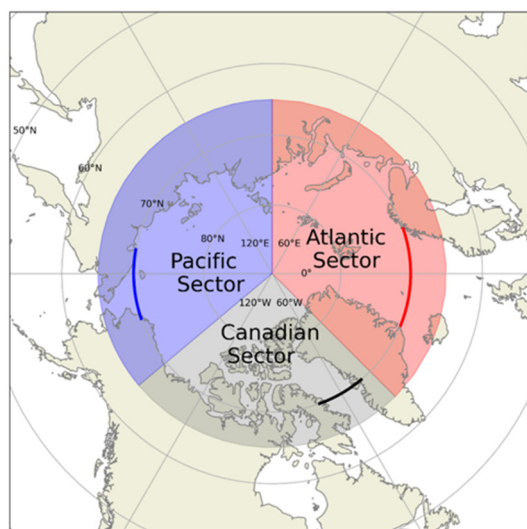


Figure 1. Schematic of the Arctic Ocean showing Pacific, Canadian, and Atlantic sectors used for box averaging. Highlighted lines show transects used to compute net freshwater fluxes across the respective sectors.

This study examines FW flux within three major parts: the Atlantic, Pacific, and Canadian sectors, associated by their distinct characteristics with adjacent water masses, fluid dynamics, and climatic parameters (Figure 1). The Atlantic sector is influenced by the inflow of warm, saline North Atlantic water through the eastern Fram Strait and the export of cold, Arctic FW through the Western Fram Strait. In contrast to the Atlantic, the Pacific Ocean provides fresher water to the Arctic through the Bering Strait inflow. Finally, the Canadian sector encompasses exchange between the CAA and the North Atlantic Ocean by the import (export) of water through the eastern (western) portion of the Davis Strait [52]. Past studies have described the complex and dynamic transports within the Arctic and

connected water pathways [15,53]. Time series of FW flux, SST, SSS, SIC, surface wind, and oceanic currents are analyzed in these regions. Transects at 70°N were selected for all three sectors to measure the flux of major ocean current passageways connecting to the Arctic.

2.2.2. Freshwater Flux Estimation

We compute surface FW flux (FW , units m^2s^{-1}) as [54]:

$$FW_{zonal} = S_{fw} \times U \times lat_{dist} \quad (1)$$

$$FW_{meridional} = S_{fw} \times V \times lon_{dist} \quad (2)$$

where the standardized (unitless) freshwater anomaly (S_{fw}) from salinity,

$$S_{fw} = (S_R - SSS) / S_R \quad (3)$$

S_R is the reference salinity 34.8 psu, the mean salinity in the Arctic region [15,55]. SSS is sea surface salinity, U is zonal surface velocity (ms^{-1}), V is meridional surface velocity (ms^{-1}), and lat_{dist} and lon_{dist} are the horizontal expanse of the data grid cells (m).

3. Results

3.1. Arctic's Mean State (2016–2018)

The Arctic's surface waters are influenced by complex atmospheric and oceanic interactions, of which the cryosphere plays an important role. Differences in SST, SSS, and SIC provide valuable insight into trends of Arctic FW flux and its connection to lower latitudes [56] (Figure 2). The warm inflow of water in the Atlantic region restricts the extent of sea ice formation as seen in Figure 2a,b. In contrast, the Pacific and Canadian sectors are colder with less saline waters, which allow sea ice to extend much further south in those regions. Regional SSS variability is pronounced by the localized increase of river discharge and net precipitation (Figure 2c,d).

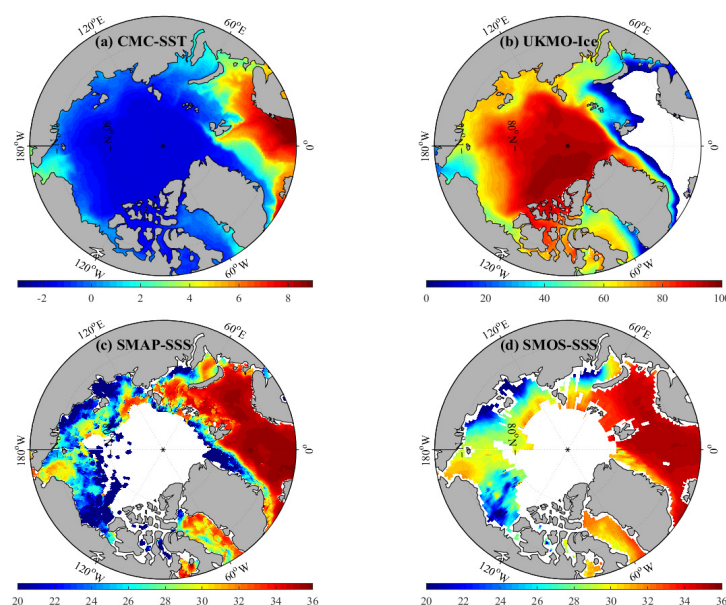


Figure 2. Annual mean (covering 2016–2018) for (a) CMC SST (°C), (b) UKMO Ice concentration (%), (c) SMAP SSS (psu), and (d) SMOS SSS (psu).

Since FW input on smaller scales is more detailed, we compare the SSS observations from SMAP and SMOS satellite data to detect the lower saline areas within the Arctic. From 2016–2018, SMAP details lower salinity gradients in Northeast Greenland, part of the CAA, and to a larger extent in the Pacific sector. SMAP also shows higher SSS extending

north across Eurasia. Both satellite missions overlap during the 2016–2018 time period and are therefore used for comparison in Figure 2. The coarser resolution of SMAP seen in Figure 2c is favored when observing mesoscale and coastal regions such as the Laptev, Kara, and Beaufort seas in the Pacific sector, the finite differences within the CAA in the Canadian sector, and along the west coast of Greenland in the Atlantic sector [41]. These areas incorporate major river mouths and edges of sea ice, which SMAP computes lower salinity gradients and contribute to the FW budget; details of which are not as well defined in SMOS. Although SMAP depicts more fine-scale changes occurring in the Arctic [40], SMOS has collected data for a longer period of time [57]; therefore, we will analyze SMOS salinity for the rest of the paper, as it contains salinity observations covering the 2010–2018 study period and has been previously used successfully in the Arctic region [58].

Ocean advection and the momentum of wind-driven circulation (Figure 3) influence the movement of these parameters and the transport of FW throughout the Arctic [10]. Atmospheric winds are weaker in the central Arctic and generally stronger near coastal regions and over major water pathways (Figure 3a–c). The strongest averaged winds between 2016–2018 occur in the southwestward movement over the Fram Strait, Bering Strait, and CAA. Currents flow with more distinct patterns especially around land masses and their adjacent ocean shelves (Figure 3d–f). The major pathways are illustrated by overall movements in Figure 3f. There is a noticeably strong current in the Laptev Sea with an average northeastward flow and another in the Beaufort Sea where the predominantly anticyclonic flow of the Beaufort Gyre occurs. Understanding the variability of SSS, SST, and SIC to the forcing of wind and currents is important when estimating the FW accumulation and pathways within the Arctic.

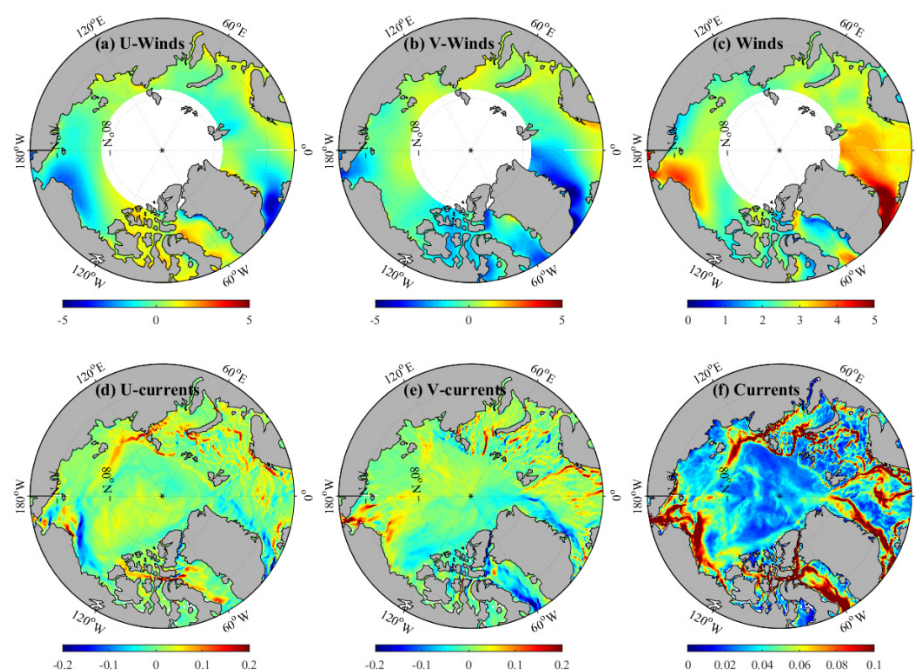


Figure 3. Annual mean (covering 2016–2018) for (a) CCMP zonal wind speed (ms^{-1}), (b) CCMP meridional wind speed (ms^{-1}), (c) CCMP wind speed magnitude (ms^{-1}) (d) ORAS5 zonal surface current speed (ms^{-1}), (e) ORAS5 meridional surface current speed (ms^{-1}) and (f) ORAS5 surface current magnitude (ms^{-1}).

3.2. Interannual Variability Time Series Analysis

We construct monthly timeseries of these parameters to examine irregularities on an interannual scale between 2010 and 2018: years encompassing the low (2012/2016) and high (2013/2014) SIEs (Figure 4). We analyze the 2010–2018 monthly interannual anomalies of SST, SIC, and SSS in Figure 5 to observe the extent of irregularities especially within

the focus years. The interannual anomalies are computed by subtracting the monthly climatologies from the monthly time series. The unavailability of SSS data, specifically in the Pacific sector, result from the limitation of satellite observations due to sea ice obstruction.

Surface waters in the Atlantic sector are overall warmer than the Pacific and Canadian sectors because of the warm Gulf stream flow brought to the high latitudes from the North Atlantic Current [59]. Low SIE years of 2012/2016 had SICs lower than 60% in all sectors (Figure 4b). The largest SIC change was more than a 20% increase between 2012 to 2013 summers in the Pacific sector. The SIC was particularly low in the Atlantic sector the same year, whereas the Canadian and Pacific sectors show greater than 5% and 10% SIC anomalies, respectively (Figure 5b). 2013 also experienced the lowest SST anomalies and higher SSS anomalies (Figure 5a,g) in the Pacific and Canadian sectors. The Canadian sector's sea ice retained roughly the same minimum concentration through 2014. The SIC in the Atlantic sector did not decrease nearly as much in 2014, whereas the Pacific sector's SIC decreased and SST increased more than the prior year. The SSS in that sector remained higher than average in 2014 than any other year during this time period. All sectors experienced positive and negative SIC anomalies in 2014 and 2016, respectively, unlike in earlier corresponding years where the Atlantic sectors did not align with a similar magnitude as the Pacific and Canadian regions (Figure 5d). By 2016 the Atlantic sector also experienced higher than average SST and SSS. There was a 10% difference in SIC in the Canadian sector between high and low SIE years.

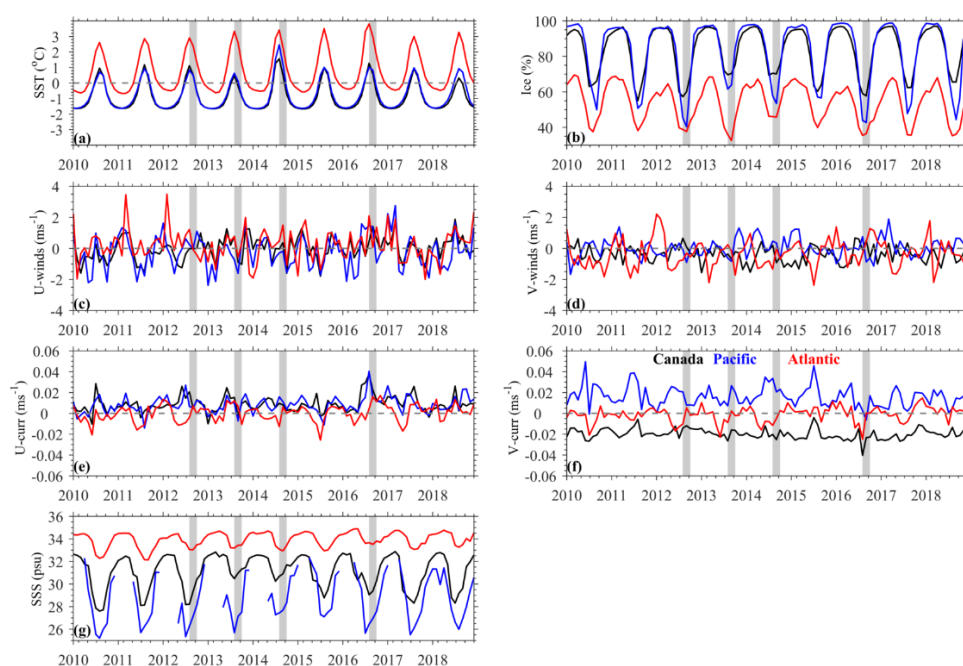


Figure 4. Box-averaged monthly time series for the Canadian (black), Pacific (blue) and Atlantic (red) sectors for (a) CMC SST ($^{\circ}\text{C}$), (b) UKMO ice concentration (%), (c) zonal winds speed (ms^{-1}), (d) meridional wind speed (ms^{-1}), (e) zonal currents (ms^{-1}), (f) meridional currents (ms^{-1}), and (g) SMOS SSS (psu). The gray-colored bands show the periods of minimum (2012/2016) and maximum (2013/2014) September sea ice extent.

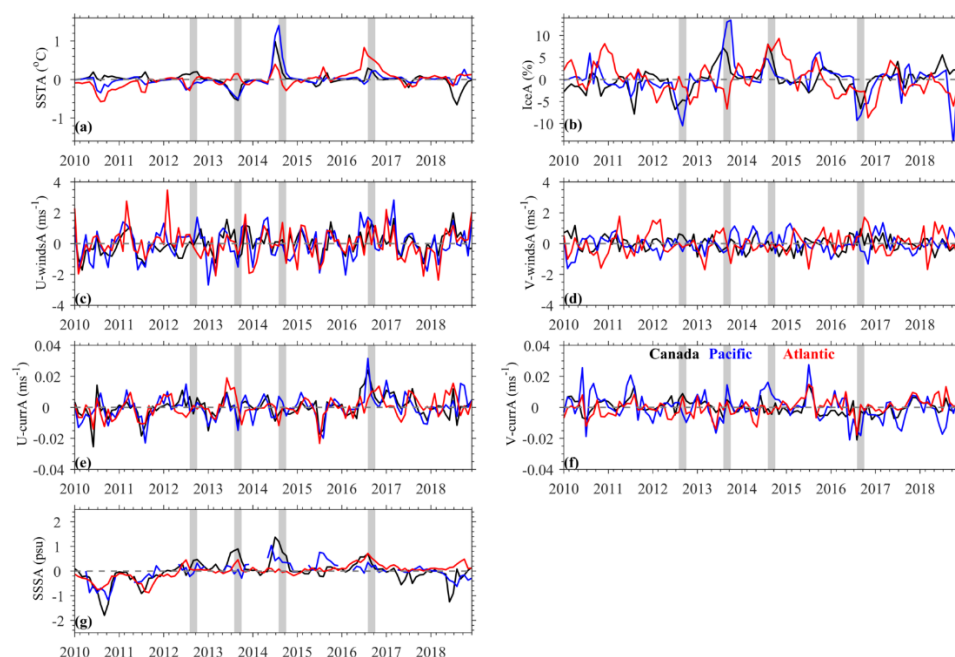


Figure 5. Box-averaged interannual anomalies time series for the Canadian (black), Pacific (blue) and Atlantic (red) sectors for (a) CMC SST ($^{\circ}\text{C}$), (b) UKMO Ice concentration (%), (c) zonal winds speed (ms^{-1}), (d) meridional wind speed (ms^{-1}), (e) zonal currents (ms^{-1}), (f) meridional currents (ms^{-1}), and (g) SMOS SSS (psu). The gray-colored bands show the periods of minimum (2012/2016) and maximum (2013/2014) September sea ice extent.

The winds (Figure 4c,d) and currents (Figure 4e,f) are quite variable on an interannual scale. General observations show that Atlantic winds are slightly stronger in the southward direction, as shown in Figure 3c, except for 2016 where there is a strong increase in northward wind flow over the summer months. Currents had the strongest eastward flow in the Pacific and Canadian sectors during the summer of 2016. Meridional currents in Figure 3f are distinguishable between sectors because of their associated inflow and outflow patterns, as discussed earlier.

3.3. Multiparameter Composite Mean Analysis

Next, we observe the geographical distributions of the interannual fluctuations between the high/low SIE years. We analyze the means of SST, SIC, and SSS between August and October to encompass the annual sea ice low that occurs in the month of September (Figure 6).

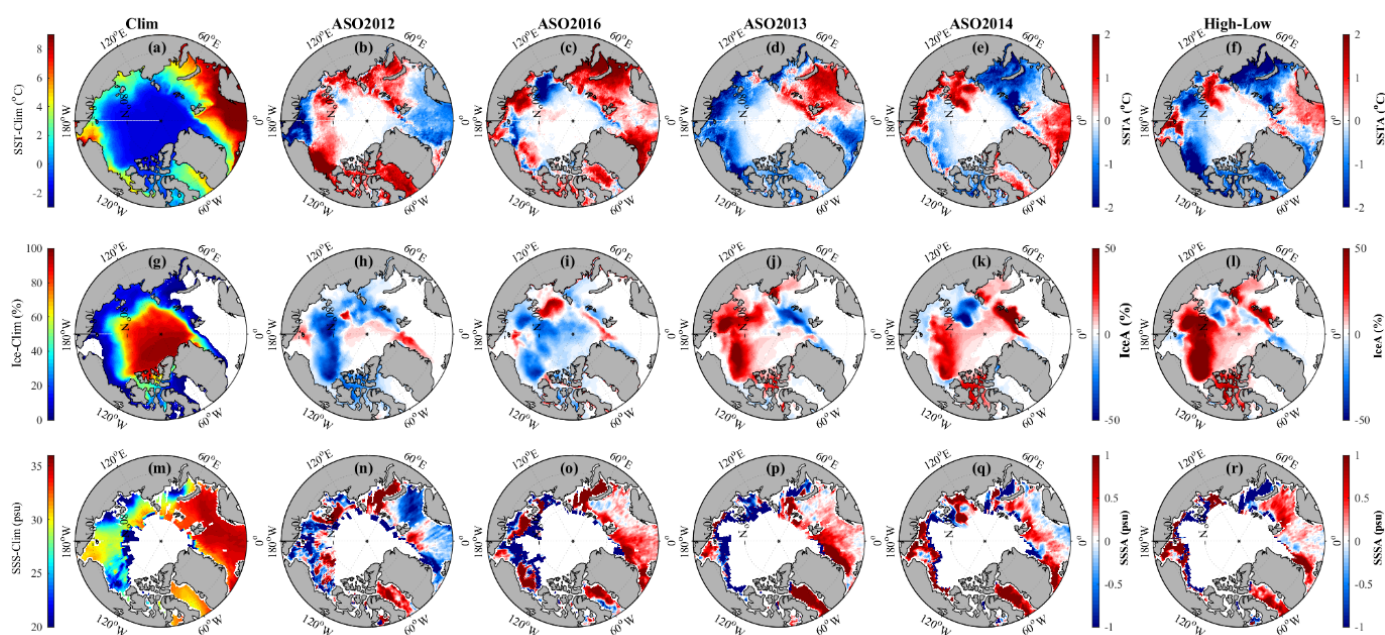


Figure 6. Composite means of August to October. First row (a–f): (a) 2010–2018 climatology of CMC SST ($^{\circ}\text{C}$). Composite means of August to October SST interannual anomalies ($^{\circ}\text{C}$) for (b) 2012, (c) 2016, (d) 2013 and (e) 2014. (f) shows the SST interannual anomalous difference between high/low SIE years (i.e., mean of (d) and (e) minus mean of (b) and (c)). Second row (g–l): as in first row but for ice concentration (%). Third row (m–r): as in first row but for SSS (psu).

In 2012, the largest warm water anomaly of more than 2°C was found close to the coast north of Alaska/Western Canada, while in 2016, a warm anomaly of similar magnitude was found in the eastern Barents Sea/Kara Sea. Overall, positive SST covers more surface area during 2012/2016. The Kara and Laptev Seas show great differences in SST magnitude and dispersal within all four years. SIE anomalies within the autumn months (Figure 6g) display the highest concentrations near the northern pole, especially north of Greenland in the Canadian sector.

To understand these parameters more precisely, the individual monthly data is also shown in Figures 7–9. SST variability is primarily strongest near the coastal regions, but the degree and spatial coverage are not as anticipated for each year (Figure 7). SST mapped in Figure 7a, and consistent with a study by Tsubouchi et al. [9], is higher near the Barents Sea (up to $\sim 9^{\circ}\text{C}$) and the Eastern Fram Strait ($\sim 7^{\circ}\text{C}$). The SST in the Bering Sea shows the high variability ($\sim -2^{\circ}\text{C}$ to 8°C). The CAA and Beaufort Sea are dominated by high SST in 2012/16 and cooler SST in 2013/2014. The Pacific sector underwent a large low SST anomaly in 2013, allowing for the recovery and retention of SIC. Overall, 2016 experienced the highest summer SST in the Bering Strait and northern Canadian regions [60]. Overall, positive SST anomaly differences are shown near the Bering Strait and Laptev Sea within the Pacific sector. In contrast, the Kara Sea in the Arctic sector and CAA in the Canadian Sector have a negative SST anomaly difference, meaning that the low-sea ice years were warmer overall in those areas.

While the averaged SICs of each section were lower in 2012/2016 than 2013/2014 as seen in Figure 5b, the spatial distribution of the sea ice varied between years where differences were most prominent north of the Bering Strait. Overall, the SIE area difference (Figure 6l) has a higher anomaly concentrated within the Pacific sector compared to the Arctic or Canadian sector.

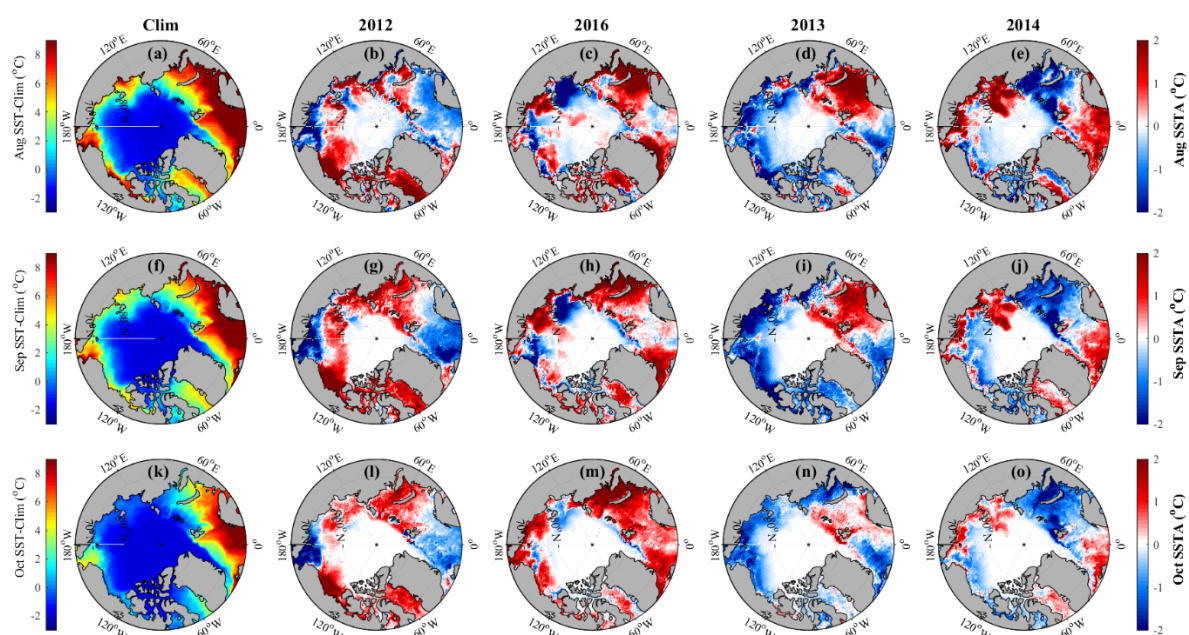


Figure 7. First row: (a) August climatology of CMC SST ($^{\circ}\text{C}$). August interannual SST anomalies ($^{\circ}\text{C}$) for (b) 2012, (c) 2016, (d) 2013 and (e) 2014. Second row: as in first row but for September. Third row: as in first row but for October.

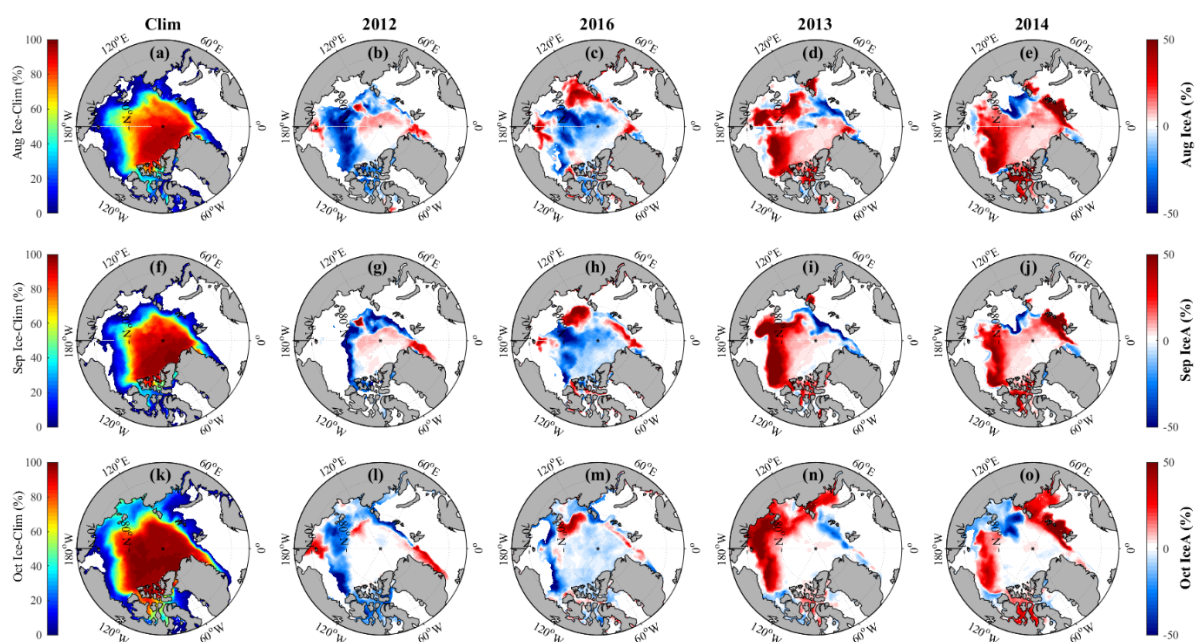


Figure 8. First row: (a) August climatology of UKMO Ice concentration (%). August interannual SIC anomalies (%) for (b) 2012, (c) 2016, (d) 2013 and (e) 2014. Second row: as in first row but for September. Third row: as in first row but for October.

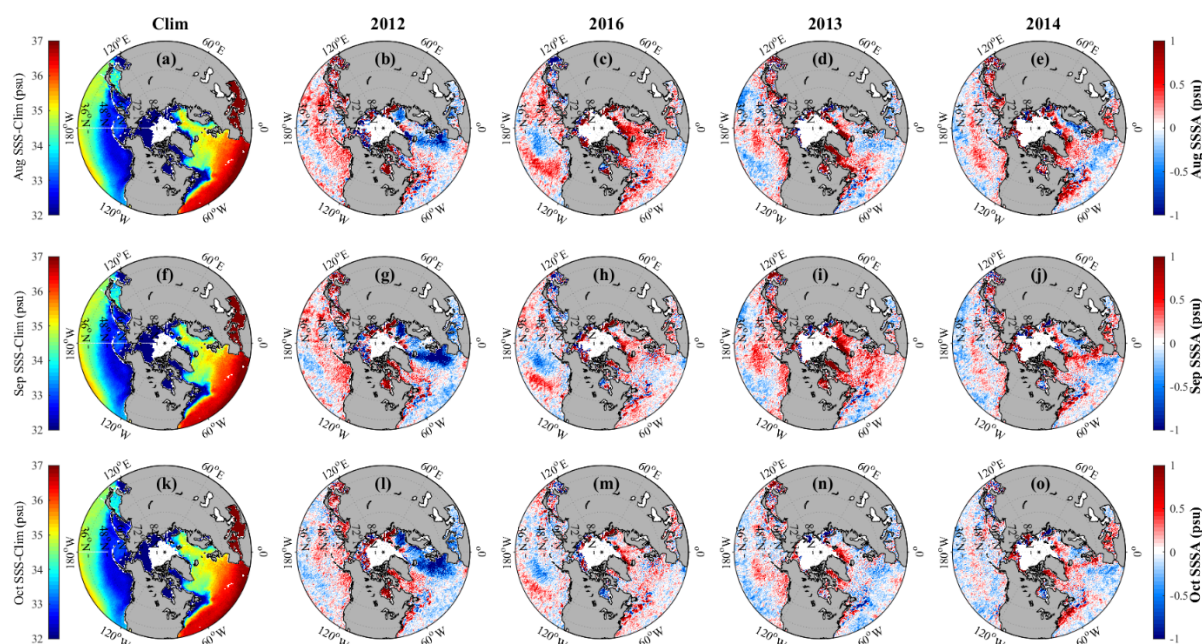


Figure 9. First row: (a) August climatology of SMOS SSS (psu). August SSS interannual anomalies (psu) for (b) 2012, (c) 2016, (d) 2013 and (e) 2014. Second row (f–j): as in first row but for September. Third row (k–o): as in first row but for October.

Next, we analyze monthly SIC discrepancies between the summer months of the high/low SIE years in Figure 8. Large variability occurs between August and September as the melt season peaks. SICs are highest north of Greenland and the CAA. Stronger anomalies occur in the Pacific sector between the focused years. SICs in 2012 were abnormally low along the sea ice perimeter, but higher near the northern pole, whereas 2016 showed slightly lower concentrations overall but higher than average concentrations north of the Laptev sea.

Since sea ice accumulates less in the Atlantic sector due to its higher SST and SSS characteristics, the retention of sea ice within the Pacific sector during the later melt months of August through October are important in determining the overall annual minimum SIE.

Areas of sea ice growth (melt) tend to decrease (increase) local SSS, making it an important parameter when observing the deduction (addition) to the FW budget (Figure 9). Adjacent oceans contribute different concentrations of salinity, showing fresher waters in the Pacific as opposed to a more saline Atlantic sector from Atlantic Ocean inflow. Since the CAA primarily experiences outflow of Arctic water, salinities vary interannually. In 2013 and 2014, more saline conditions were concentrated around Greenland in the Canadian/Atlantic sectors. This compares well with Figure 5, which shows the Canadian sector having the highest SSS in the years of high SIE.

FW flux between the Arctic and the sector transects primarily travel north, into the Arctic or south, away from the Arctic; therefore, we compute the meridional transport instead across these sections (Figure 10). Due to the Bering Strait inflow, the Pacific sector experiences a higher FW flux compared to the Atlantic sector's balanced transports and the Canadian sectors' outflow [8]. The largest export of FW in the Atlantic sector occurs in 2012 (Figure 10a), a time when the Pacific sector experiences an anomalously low import of FW (Figure 10b).

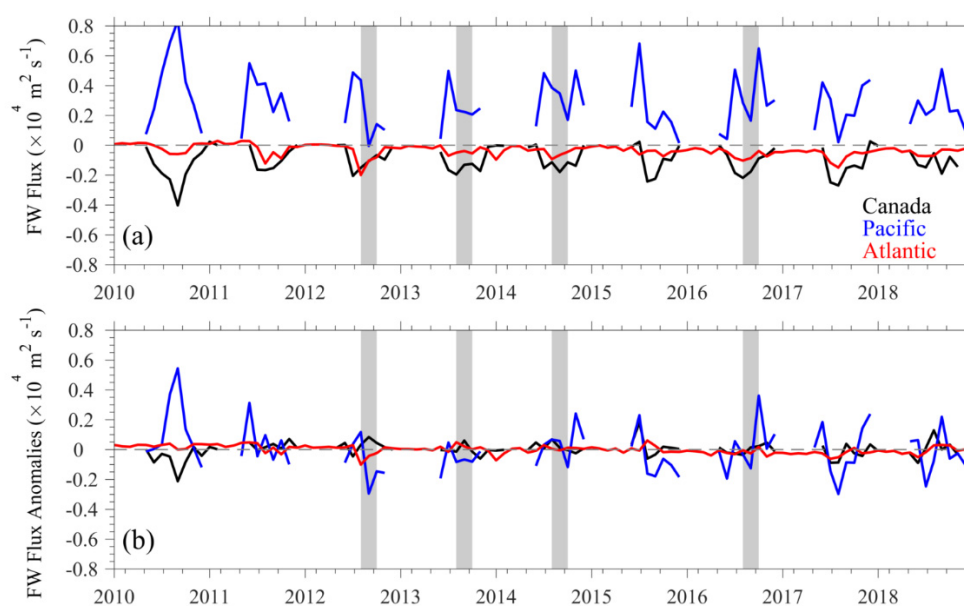


Figure 10. (a) Monthly net meridional FW fluxes (m^2s^{-1}), and (b) interannual anomalies of net meridional FW fluxes (m^2s^{-1}) across 70°N in the Canadian (black), Pacific (blue), and Atlantic (red) sectors. The gray-colored bands show the periods of minimum (2012/2016) and maximum (2013/2014) sea ice extent.

3.4. Atlantic Freshwater Pathways

The FW outflow from the Arctic Ocean into the North Atlantic incorporates numerous pathways, many of which oppose each other, i.e., the northeast Barents Sea Opening (BSO) flow and the southwest Fram Strait current. Therefore, we analyze the dominant flux pathways in the Arctic sector separately (Figure 11). Two pathways connecting the Atlantic and Arctic Ocean are the BSO and the Fram Strait (Figure 11a). A third transect is computed to capture the low anomalous salinity event in the summer to fall of 2012, hereafter referred to as the northeast Atlantic section (NEA) (Figure 11a).

Dominant movement through the BSO flows in the zonal direction, while the Fram Strait and the NEA experience predominantly meridional flows; therefore, we computed FW flux in the transects to their respective directional transport (Figure 11b,c). Fluctuations in transport depend on atmospheric processes driving currents through these sectors, with no obvious seasonal oscillations over the regional areas. As seen in Figure 11, October 2012 has a high FW flux through the NEA transect equating to $0.32 \times 10^3 \text{ m}^2\text{s}^{-1}$ which has a positive anomalous FW flux of $0.47 \times 10^3 \text{ m}^2\text{s}^{-1}$. In the summer of 2012, the Fram Strait and BSO have their highest FW flux at $0.12 \times 10^3 \text{ m}^2\text{s}^{-1}$ and $0.10 \times 10^3 \text{ m}^2\text{s}^{-1}$ respectively.

The general trend of the FW flux through the Fram Strait decreases at a monthly rate of $6.0 \text{ m}^2\text{s}^{-1}$ from 2010–2018, with a more recent declining monthly trend of $10 \text{ m}^2\text{s}^{-1}$ from 2015–2018. This is especially true during 2017 and 2018 where a drastic negative FW flux occurs, opposed to the positive flux through the NEA transect (Figure 11b,c). Higher SSS are alongside the eastern Greenland coast in 2013, causing its lower FW flux anomalies through the Fram Strait. A larger salinity gradient passes through the NEA transect in the summer of 2014 as shown in Figure 9j and computed in Figure 11c. Quantifying the FW flow specifically within these three transects distinguishes the Arctic's contribution to the North Atlantic and vice versa; especially as annual conditions change towards a warmer, northern climate regime.

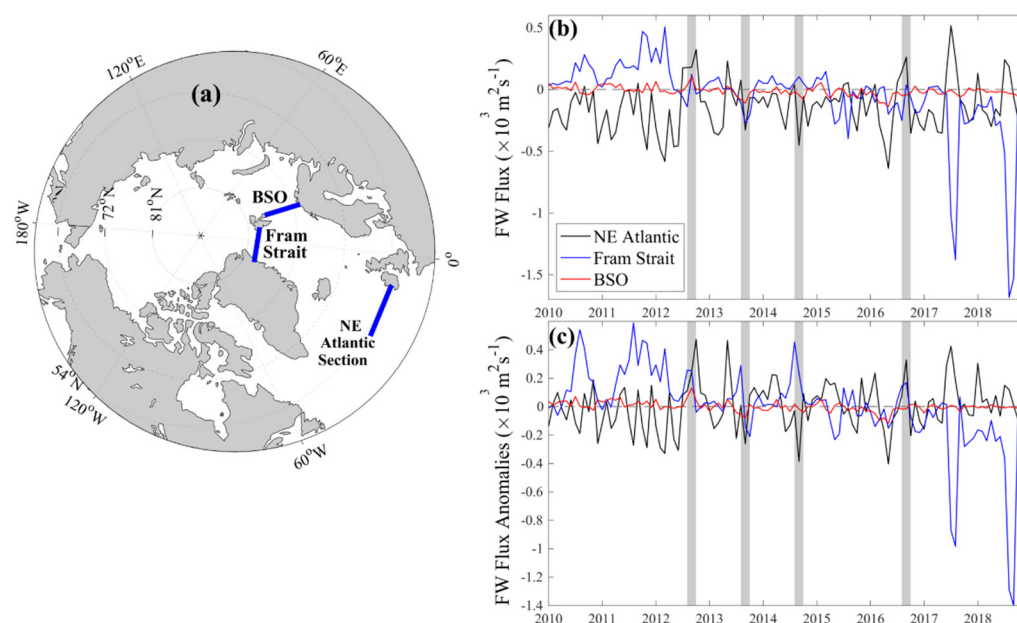


Figure 11. (a) A schematic of the Arctic Ocean showing the Northeast (NE) Atlantic Section (53°N, 10°W to 25°W), Fram Strait (79°N, 11°E to 19°W), Barents Sea Opening (BSO) (71°N to 77°N, 23°E) with corresponding (b) FW Flux and (c) FW Flux interannual anomalies (m^2s^{-1}) during 2010–2018. Meridional flux was computed for NE Atlantic and Fram Strait sections, while zonal flux was computed for the BSO as the dominant movements. The gray-colored bands show the periods of minimum (2012/2016) and maximum (2013/2014) September sea ice extent.

4. Discussion

4.1. Multiparameter Variability in Extreme SIE Years

4.1.1. SST, SSS, SIC

SIE retains its highest extent between March and April, while retreating to its lowest extent by September or August depending on the threshold of SIC used, typically greater than or equal to 15% [19]. We observe climatic trends through years of low (2012/2016) and high (2013/2014) SIE and associations between parameters of SST and SSS that attribute to their SIC extremes. We also delineate monthly patterns in the summers of those years which influence the transport of FW between the Arctic and subarctic regions. Brown et al. [12] describes precipitation to have less of an input to the Arctic's FW storage, but more complexity when quantifying. This study features the recent SSS Arctic state through SMOS satellite data in relation to other parameters between 2010 and 2018. SSS was greater in the high SIE years, especially in the Canadian sector where higher concentrations of sea ice retained the fresher waters.

Interannual variability of SST influenced the low SIE of 2012/2016 as warmer areas intensified throughout the Arctic while 2013/2014 showed overall cooling through each month observed. SST varied within different Arctic seas, governing the conditions for sea ice formation. Although low on average, regional Arctic SST is increasing annually which can obstruct the formation of winter sea ice and the retention of multi-year sea ice during the summer. Anomalous warm SST in 2012 and 2016 occurred especially in the Barents and Kara seas, which Jung et al. [61] credited to the influence of eddy transport and retention.

The Atlantic sector experienced the lowest SIC during 2013, while the Pacific and Canadian sectors remained high. This has been attributed to a strong warm temperature anomaly in the Barents Sea as well as an overall negative sea level pressure, which suggests the lower sea ice melt and higher SSS compared to the other sectors [22]. 2014 showed anomalously high SST during the early summer despite its retention of SIC in all sectors, especially the Atlantic, which was lower than normal the year prior. Di Lorenzo et al. [62]

examined a marine heatwave in 2014 in the North Pacific that created the anomalous high SST entering the Arctic through the Bering Strait mainly fed by atmospheric forcing. High SSTA from the Pacific sector in 2016 matches the studies from Hu et al. [63] and Hartmann [64] that investigated the influentially strong, warm phase of the El Niño Southern Oscillation (ENSO) of that year. This induced warmer SSTs in the northeast Pacific Ocean, curating warmer surface temperatures through the Bering Strait from oceanic heat loss and weak, cold water advection to the upper ocean during 2016.

The summer of 2014 also experienced a higher than normal SIC, shown by late melting and early freeze onset days [65]. Sea ice accumulates highest North of Greenland and the CAA aided by anticyclonic wind from the Beaufort Sea; however, Petty et al. [65] describes melt and freeze onset days throughout this time period that could contribute to the levels of SIC seen in this study. Earlier melt onset days in 2012/2016 hindered the chance for sea ice to accumulate over the fall months. Faster sea ice melt quickens the pace of FW release back to the ocean surface and the interaction to the atmosphere or oceanic fluid dynamics. Melt onset days started at consistent times in 2013/2014; however, in 2013, an early freeze onset was recorded in the Eastern Arctic, comparing well to that of high concentrations that October. There was a later freeze onset in 2016, restricting its ability to store as much ice, which correlates well to the total lower sea ice anomalies spread throughout the sea ice area of that year. Ricker et al. [43] also pointed that the inability to sustain multiyear sea ice caused unfavorable conditions for the increase of SIC in 2016, matching our observations of lower SIC overall. The preservation of thick sea ice over winter months, specifically from the northwest part of Greenland, permitted a higher minimum SIE for 2013 and 2014 [66]. Comiso et al. [17] expresses the implications that pre-conditioning warming has on the following years' SIE. Increased present and near-future atmospheric warming will impede the ability for sea ice to remain throughout the summer months.

4.1.2. Winds and Currents

Atmospheric forcing plays a significant role on the direct contact with the ocean surface interface and governs the intensity of water transport. Winds also influence deep convection, especially in the North Atlantic Meridional Overturning Circulation (AMOC). Ocean current direction and magnitude are driven by atmospheric wind forcing, both of which modify sea ice content and drift [67]. For example, storm forcing in 2012 caused prominent variations, leading towards changes in the Beaufort Sea where the spatial distribution of SIC varies [68]. Summer sea ice especially increased in the Beaufort Sea from 2012 to 2013 (Figure 6j), which Liu and Key [23] attributed to the decrease in winter cloud cover. Future research can incorporate the effects of higher atmospheric conditions to SIC and subsequently the relationship to FW flux. The 33% SIE increase from September of 2013 to 2012 was mainly attributed to the retention of sea ice and accumulation driven by atmospheric forcing [66].

Meridional currents in each sector are most distinguishable between the Arctic and subarctic regions where the Pacific sector has a constant northward current that flows into the Arctic while the dominant current in the Canadian sector is southward, out of the Arctic. The meridional current in the Atlantic sector is balanced by the inflow of water to the Arctic through the Barents Sea and the east side of the Fram Strait with a substantial southward flow out of the Arctic on the west side of the Fram Strait [9]. A strong, wide current is also observed within the Arctic in the north Laptev sea, one of the first areas to begin the growth of winter sea ice every year [28]. The extent of this study observes currents flowing into the Arctic from subarctic regions; future studies can incorporate the movement of water flow solely within the Arctic. Currents in 2016 had a greater southwestward movement in the Pacific and Canadian sectors than usual. Overland et al. [69] suggests an eastern shift of winds driven by the midlatitudes caused the lowest February temperatures in 2016, with a 2 °C warmer anomaly, preconditioning thinner and more mobile ice compared to the earlier years of the 2010s [35]. Increased winds and current drift speeds could result in a higher sea ice or liquid FW transport out of the Arctic.

4.2. Freshwater Fluxes

An averaged negative FW flux occurs in the Atlantic and Canadian Sectors while a positive FW flux is prominent in the Pacific Sector. However, there are large variations in the interannual anomalies of meridional FW flux throughout the Arctic. Years of low SIE seem to vary primarily in the Pacific Sector which can be attributed to the predominant, anticyclonic movement of the Beaufort Gyre circulating FW to diverging regions [70]. With an earlier melt season, outflow of FW in 2016 occurred at a higher magnitude in the Canadian Sector as opposed to an export through the Eastern Greenland Current (EGC). Dodd et al. [71] assigns the EGC responsible for exporting between $1/2$ to $3/4$ of the Arctic's sea ice and liquid FW to the North Atlantic, where interaction with the Nordic seas can impact the overturning of North Atlantic surface waters important for the AMOC. Jahn et al. [72] observed FW in sea ice is exported primarily through the Fram Strait in the Atlantic sector while larger liquid FW is generally expelled through the CAA.

A significantly notable surface FW anomaly in 2012 passed in the East Greenland Current (EGC) through the Denmark Strait, of which explanations are still not well illustrated [73]. Therefore, we observed the implications of subpolar FW transport in the North Atlantic Ocean.

4.3. Atlantic Freshwater Pathways

Compared to the Pacific and Canadian sectors, the Atlantic sector incorporates various flow directions and cannot be accurately characterized by one transect. Skliris et al. [74] observed up to a 20% increase within the last 40 years of average meridional FW export from the Arctic to the North Atlantic Ocean, an area that depends on weaker stratification for thermohaline circulation. In order to understand the contribution of FW inflow and dispersion of outflow, we observed freshwater fluxes through three separate transects in the Atlantic region.

A low salinity anomaly occurred in 2012 where about a 75% larger FW transport was exported into the Atlantic Sector unlike that of its shared low SIE year of 2016 [73]. De Steur et al. [75] described high FW transport anomalies within July 2012, most likely continuing FW export through the EGC as seen in Figure 9. Nghiem et al. [76] attributed the decrease in adjacent surface salinity of Greenland to the anomalously large melt across 98% of the ice sheet most likely due to a warm ridged air interaction. However, it is still uncertain to what parameters or their contribution to the abnormal FW outflow away from Greenland. We explore this unusual surface FW event further in Figure 11.

Sea ice export through the Fram Strait declined between 1991 and 2010, whereas southward FW flux has increased about 49% from the 1959–1990 average in the southeast of Greenland [77]. Josey et al. [78] suggests that other contributions to the fresher NEA region is from net precipitation and pressure gradient of NAO. The more likely factor is a change in the East Atlantic Pattern, which is similar to the NAO but with a southward shift. FW flux through the NEA is higher in both years of low SIE, suggesting FW export effects from the Arctic on mid-latitudes. As low SIE years become more dominant, FW flux into the North Atlantic could change the AMOC drastically if prompted by enough Arctic FW, changing the global thermohaline circulation. Therefore, incorporating FW observations from precipitation and river input with Arctic FW export when observing changing SSS will improve the knowledge of polar region influence on the global circulation.

5. Conclusions

The Arctic's cold, FW budget is a driving factor to the strength of the polar halocline and the slowdown of the overturning advection in the north AMOC, despite its relatively small surface area. A seasonal contributor for increased FW is Arctic sea ice with lowest extents at the end of the melt season in September. In the last decade, there is a general decreasing trend of annual SIE due to Arctic Amplification as a consequence of anthropogenic induced climate change primarily induced by greenhouse gas emissions [28]; however, the yearly variations of these extents are still unknown. From this study, we

utilize remote sensing data and model outputs to examine the transport and variability of climatic parameters in the Arctic and interconnected spatiotemporal ranges.

With box-averages of each sector we described the major contributions of adjacent seas and Arctic characteristics, then focused on the multiparameter variations within the individual years of low and high sea ice extent. There we specified trends in different regions through the scope of the summer seasons where large fluctuation occurred in the Laptev, Kara, and Barents seas. We observed an anomalous surface FW transport event in the subarctic and the North Atlantic regions in 2012. Past studies mention the possible contribution of the increasing annual declination of the southeastern Greenland ice sheet [34,46,52].

Models and satellites allow us to estimate parameters where in situ instruments lack, especially in harsh conditions that polar climates bring. However, there are limitations within validity of model estimations and satellite radiometer's sensitivity to colder temperatures [38]. Future work should focus on the contribution of FW through precipitation and river input and the possible implications that the Greenland Ice sheet melt has on the FW exchange with the Arctic and subarctic regions, especially on the impacts of SIE. Annual sea ice declination and FW increase within the Arctic are of major importance to understanding and predicting the polar regime.

Author Contributions: Conceptualization, B.S.; methodology, S.B.H. and E.S.N.; software, S.B.H. and E.S.N.; validation, B.S., S.B.H. and E.S.N.; formal analysis, S.B.H., B.S., E.S.N. and A.S.; investigation, S.B.H., B.S., E.S.N. and A.S.; resources, B.S.; data curation, B.S. and E.S.N.; writing, S.B.H., B.S., E.S.N. and A.S.; visualization, S.B.H., B.S., E.S.N. and A.S.; supervision, B.S.; funding acquisition, B.S. All authors have read and agreed to the published version of the manuscript.

Funding: This research was funded by the United States Office of Naval Research Awarded #N00014-20-1-2680, awarded to B.S.

Data Availability Statement: Daily OISST were obtained from NOAA/OAR/ESRL PSL and are available in 0.25° horizontal resolution from 1981–present (<https://psl.noaa.gov/data/gridded/data.noaa.oisst.v2.highres.html>) accessed on: 29 January 2021. OSTIA sea ice concentration data were taken from the EUMETSAT OSI-SAF and are available at 0.05° and are available from 2007–present (https://resources.marine.copernicus.eu/?option=com_csw&view=details&product_id=SST_GLO_SST_L4_REP_OBSERVATIONS_010_011) accessed on: 18 December 2020. SMOSv5 SSS data were taken from CATDS as a monthly 0.2° product and are available from 2010–2020 (<https://www.catds.fr/Products/Available-products-from-CEC-OS/CEC-Locean-L3-Debiased-v5>) accessed on: 16 December 2020. Monthly SMAP CAP V5.0 data were taken from NASA/JPL PO.DAAC Drive at 0.25° horizontal resolution from 2015–2020 (<https://podaac-tools.jpl.nasa.gov/drive/files/SalinityDensity/smap/L3/JPL/V5.0/monthly>) accessed on: 13 December 2020. ORAS5 ocean current data were taken from the University of Hamburg at 0.25° and are available from 1993–2019 (https://resources.marine.copernicus.eu/?option=com_csw&view=details&product_id=GLOBAL_REANALYSIS_PHY_001_031) accessed on: 13 December 2020. CCMPv2.0 near real time surface winds were obtained from RSS as a 6-h product at 0.25° horizontal resolution and are available from 1988–present (<http://www.remss.com/measurements/ccmp/>) accessed on: 30 March 2021.

Acknowledgments: We are thankful for the helpful comments of the three anonymous reviewers which improved the quality of this paper.

Conflicts of Interest: The authors declare no conflict of interest.

References

1. Walsh, J.E.; Overland, J.E.; Groisman, P.Y.; Rudolf, B. Ongoing Climate Change in the Arctic. *Ambio* **2011**, *40* (Suppl. 1), 6–16. [CrossRef]
2. Serreze, M.C.; Barry, R.G. Processes and Impacts of Arctic Amplification: A Research Synthesis. *Glob. Planet. Chang.* **2011**, *77*. [CrossRef]
3. Madhusoodanan, M.S.; Thompson, B. Decadal Variability of the Arctic Ocean Thermal Structure. *Ocean Dyn.* **2011**, *61*. [CrossRef]
4. Serreze, M.C.; Barrett, A.P.; Stroeve, J.C.; Kindig, D.N.; Holland, M.M. The Emergence of Surface-Based Arctic Amplification. *Cryosphere* **2009**, *3*. [CrossRef]

5. Yang, Q.; Dixon, T.H.; Myers, P.G.; Bonin, J.; Chambers, D.; van den Broeke, M.R. Recent Increases in Arctic Freshwater Flux Affects Labrador Sea Convection and Atlantic Overturning Circulation. *Nat. Commun.* **2016**, *7*. [\[CrossRef\]](#)
6. Rabe, B.; Karcher, M.; Kauker, F.; Schauer, U.; Toole, J.M.; Krishfield, R.A.; Pisarev, S.; Kikuchi, T.; Su, J. Arctic Ocean Basin Liquid Freshwater Storage Trend 1992–2012. *Geophys. Res. Lett.* **2014**, *41*, 961–968. [\[CrossRef\]](#)
7. Wang, Q.; Wekerle, C.; Danilov, S.; Sidorenko, D.; Koldunov, N.; Sein, D.; Rabe, B.; Jung, T. Recent Sea Ice Decline Did Not Significantly Increase the Total Liquid Freshwater Content of the Arctic Ocean. *J. Clim.* **2019**, *32*, 15–32. [\[CrossRef\]](#)
8. Woodgate, R.A. Revising the Bering Strait Freshwater Flux into the Arctic Ocean. *Geophys. Res. Lett.* **2005**, *32*. [\[CrossRef\]](#)
9. Tsubouchi, T.; Bacon, S.; Aksenov, Y.; Naveira Garabato, A.C.; Beszczynska-Möller, A.; Hansen, E.; de Steur, L.; Curry, B.; Lee, C.M. The Arctic Ocean Seasonal Cycles of Heat and Freshwater Fluxes: Observation-Based Inverse Estimates. *J. Phys. Oceanogr.* **2018**, *48*. [\[CrossRef\]](#)
10. Timmermans, M.; Marshall, J. Understanding Arctic Ocean Circulation: A Review of Ocean Dynamics in a Changing Climate. *J. Geophys. Res. Ocean.* **2020**, *125*. [\[CrossRef\]](#)
11. McClelland, J.W.; Holmes, R.M.; Dunton, K.H.; Macdonald, R.W. The Arctic Ocean Estuary. *Estuaries Coasts* **2012**, *35*. [\[CrossRef\]](#)
12. Brown, N.J.; Nilsson, J.; Pemberton, P. Arctic Ocean Freshwater Dynamics: Transient Response to Increasing River Runoff and Precipitation. *J. Geophys. Res. Ocean.* **2019**, *124*. [\[CrossRef\]](#)
13. Weatherly, J.W.; Walsh, J.E. The Effects of Precipitation and River Runoff in a Coupled Ice-Ocean Model of the Arctic. *Clim. Dyn.* **1996**, *12*. [\[CrossRef\]](#)
14. Wang, Q.; Wekerle, C.; Danilov, S.; Koldunov, N.; Sidorenko, D.; Sein, D.; Rabe, B.; Jung, T. Arctic Sea Ice Decline Significantly Contributed to the Unprecedented Liquid Freshwater Accumulation in the Beaufort Gyre of the Arctic Ocean. *Geophys. Res. Lett.* **2018**, *45*, 4956–4964. [\[CrossRef\]](#)
15. Haine, T.W.N.; Curry, B.; Gerdes, R.; Hansen, E.; Karcher, M.; Lee, C.; Rudels, B.; Spreen, G.; de Steur, L.; Stewart, K.D.; et al. Arctic Freshwater Export: Status, Mechanisms, and Prospects. *Glob. Planet. Chang.* **2015**, *125*. [\[CrossRef\]](#)
16. Yadav, J.; Kumar, A.; Mohan, R. Dramatic Decline of Arctic Sea Ice Linked to Global Warming. *Nat. Hazards* **2020**, *103*. [\[CrossRef\]](#)
17. Comiso, J.C.; Parkinson, C.L.; Gersten, R.; Stock, L. Accelerated Decline in the Arctic Sea Ice Cover. *Geophys. Res. Lett.* **2008**, *35*. [\[CrossRef\]](#)
18. Serreze, M.C.; Stroeve, J.; Barrett, A.P.; Boisvert, L.N. Summer Atmospheric Circulation Anomalies over the Arctic Ocean and Their Influences on September Sea Ice Extent: A Cautionary Tale. *J. Geophys. Res.* **2016**, *121*, 11463–11485. [\[CrossRef\]](#)
19. Matthews, J.L.; Peng, G.; Meier, W.N.; Brown, O. Sensitivity of Arctic Sea Ice Extent to Sea Ice Concentration Threshold Choice and Its Implication to Ice Coverage Decadal Trends and Statistical Projections. *Remote Sens.* **2020**, *12*, 807. [\[CrossRef\]](#)
20. Parkinson, C.L.; Cavalieri, D.J. Arctic Sea Ice Variability and Trends, 1979–2006. *J. Geophys. Res.* **2008**, *113*. [\[CrossRef\]](#)
21. Michon, S. Arctic Sea Ice Minimum Second Lowest on Record | NOAA Climate.gov. 2020. Available online: <https://www.climate.gov/news-features/featured-images/2020-arctic-sea-ice-minimum-second-lowest-record> (accessed on 19 February 2021).
22. Francis, J.A.; Wu, B. Why Has No New Record-Minimum Arctic Sea-Ice Extent Occurred since September 2012? *Environ. Res. Lett.* **2020**. [\[CrossRef\]](#)
23. Liu, Y.; Key, J.R. Less Winter Cloud Aids Summer 2013 Arctic Sea Ice Return from 2012 Minimum. *Environ. Res. Lett.* **2014**, *9*. [\[CrossRef\]](#)
24. Perovich, D.; Meier, W.; Tschudi, M.; Farrell, S.; Gerland, S.; Hendricks, S.; Krumpen, T.; Haas, C. Sea Ice. Available online: <https://www.arctic.noaa.gov/Report-Card/Report-Card-2016/ArtMid/5022/ArticleID/286/Sea-Ice> (accessed on 19 February 2021).
25. Praetorius, S.; Rugenstein, M.; Persad, G.; Caldeira, K. Global and Arctic Climate Sensitivity Enhanced by Changes in North Pacific Heat Flux. *Nat. Commun.* **2018**, *9*. [\[CrossRef\]](#) [\[PubMed\]](#)
26. Perovich, D.K.; Richter-Menge, J.A. Loss of Sea Ice in the Arctic. *Annu. Rev. Mar. Sci.* **2009**, *1*. [\[CrossRef\]](#)
27. Fournier, S.; Lee, T.; Wang, X.; Armitage, T.W.K.; Wang, O.; Fukumori, I.; Kwok, R. Sea Surface Salinity as a Proxy for Arctic Ocean Freshwater Changes. *J. Geophys. Res. Ocean.* **2020**, *125*. [\[CrossRef\]](#)
28. Kim, K.Y.; Hamlington, B.D.; Na, H.; Kim, J. Mechanism of Seasonal Arctic Sea Ice Evolution and Arctic Amplification. *Cryosphere* **2016**, *10*, 2191–2202. [\[CrossRef\]](#)
29. Harms, I.H.; Karcher, M.J. Kara Sea Freshwater Dispersion and Export in the Late 1990s. *J. Geophys. Res.* **2005**, *110*. [\[CrossRef\]](#)
30. Kodaira, T.; Waseda, T.; Nose, T.; Inoue, J. Record High Pacific Arctic Seawater Temperatures and Delayed Sea Ice Advance in Response to Episodic Atmospheric Blocking. *Sci. Rep.* **2020**, *10*. [\[CrossRef\]](#)
31. Davis, P.E.D.; Lique, C.; Johnson, H.L.; Guthrie, J.D. Competing Effects of Elevated Vertical Mixing and Increased Freshwater Input on the Stratification and Sea Ice Cover in a Changing Arctic Ocean. *J. Phys. Oceanogr.* **2016**, *46*, 1531–1553. [\[CrossRef\]](#)
32. Giles, K.A.; Laxon, S.W.; Ridout, A.L.; Wingham, D.J.; Bacon, S. Western Arctic Ocean Freshwater Storage Increased by Wind-Driven Spin-up of the Beaufort Gyre. *Nat. Geosci.* **2012**, *5*. [\[CrossRef\]](#)
33. Wang, Z.; Hamilton, J.; Su, J. Variations in Freshwater Pathways from the Arctic Ocean into the North Atlantic Ocean. *Prog. Oceanogr.* **2017**, *155*, 54–73. [\[CrossRef\]](#)
34. Morison, J.; Kwok, R.; Peralta-Ferriz, C.; Alkire, M.; Rigor, I.; Andersen, R.; Steele, M. Changing Arctic Ocean Freshwater Pathways. *Nature* **2012**, *481*, 66–70. [\[CrossRef\]](#) [\[PubMed\]](#)
35. Kwok, R.; Spreen, G.; Pang, S. Arctic Sea Ice Circulation and Drift Speed: Decadal Trends and Ocean Currents. *J. Geophys. Res. Ocean.* **2013**, *118*, 2408–2425. [\[CrossRef\]](#)

36. Wang, Q.; Ricker, R.; Mu, L. Arctic Sea Ice Decline Preconditions Events of Anomalously Low Sea Ice Volume Export through Fram Strait in the Early 21st Century. *J. Geophys. Res. Ocean.* **2021**. [\[CrossRef\]](#)
37. Stroh, J.N.; Panteleev, G.; Kirillov, S.; Makhotin, M.; Shakhova, N. Sea-Surface Temperature and Salinity Product Comparison against External In Situ Data in the Arctic Ocean. *J. Geophys. Res. Ocean.* **2015**, *120*, 7223–7236. [\[CrossRef\]](#)
38. Lang, R.; Zhou, Y.; Utku, C.; le Vine, D. Accurate Measurements of the Dielectric Constant of Seawater at L Band. *Radio Sci.* **2016**, *51*. [\[CrossRef\]](#)
39. Fournier, S.; Lee, T.; Tang, W.; Steele, M.; Olmedo, E. Evaluation and Intercomparison of SMOS, Aquarius, and SMAP Sea Surface Salinity Products in the Arctic Ocean. *Remote Sens.* **2019**, *11*, 43. [\[CrossRef\]](#)
40. Tang, W.; Yueh, S.; Yang, D.; Fore, A.; Hayashi, A.; Lee, T.; Fournier, S.; Holt, B. The Potential and Challenges of Using Soil Moisture Active Passive (SMAP) Sea Surface Salinity to Monitor Arctic Ocean Freshwater Changes. *Remote Sens.* **2018**, *10*, 869. [\[CrossRef\]](#)
41. Lind, S.; Ingvaldsen, R.B.; Furevik, T. Arctic Warming Hotspot in the Northern Barents Sea Linked to Declining Sea-Ice Import. *Nat. Clim. Chang.* **2018**, *8*, 634–639. [\[CrossRef\]](#)
42. Kedra, M.; Moritz, C.; Choy, E.S.; David, C.; Degen, R.; Duerksen, S.; Ellingsen, I.; Górska, B.; Grebmeier, J.M.; Kirievskaya, D.; et al. Status and Trends in the Structure of Arctic Benthic Food Webs. *Polar Res.* **2015**, *34*. [\[CrossRef\]](#)
43. Ricker, R.; Hendricks, S.; Girard-Ardhuin, F.; Kaleschke, L.; Lique, C.; Tian-Kunze, X.; Nicolaus, M.; Krumpen, T. Satellite-Observed Drop of Arctic Sea Ice Growth in Winter 2015–2016. *Geophys. Res. Lett.* **2017**, *44*, 3236–3245. [\[CrossRef\]](#)
44. Polyakov, I.V.; Pnyushkov, A.V.; Carmack, E.C. Stability of the Arctic Halocline: A New Indicator of Arctic Climate Change. *Environ. Res. Lett.* **2018**, *13*. [\[CrossRef\]](#)
45. Chao, Y.; Li, Z.; Farrara, J.D.; Hung, P. Blending Sea Surface Temperatures from Multiple Satellites and In Situ Observations for Coastal Oceans. *J. Atmos. Ocean. Technol.* **2009**, *26*. [\[CrossRef\]](#)
46. Prange, M.; Gerdes, R. The Role of Surface Freshwater Flux Boundary Conditions in Arctic Ocean Modelling. *Ocean Model.* **2006**, *13*. [\[CrossRef\]](#)
47. Boutin, J.; Vergely, J.L.; Marchand, S.; D'Amico, F.; Hasson, A.; Kolodziejczyk, N.; Reul, N.; Reverdin, G.; Vialard, J. New SMOS Sea Surface Salinity with Reduced Systematic Errors and Improved Variability. *Remote. Sens. Environ.* **2018**, *214*. [\[CrossRef\]](#)
48. Fore, A.G.; Yueh, S.H.; Tang, W.; Stiles, B.W.; Hayashi, A.K. Combined Active/Passive Retrievals of Ocean Vector Wind and Sea Surface Salinity With SMAP. *IEEE Trans. Geosci. Remote Sens.* **2016**, *54*, 7396–7404. [\[CrossRef\]](#)
49. Wentz, F.J.; Scott, J.; Hoffman, R.; Leidner, M.; Atlas, R.; Ardizzone, J. Remote Sensing Systems Cross-Calibrated Multi-Platform (CCMP) 6-Hourly Ocean Vector Wind Analysis Product on 0.25 Deg Grid, Version 2.0. Remote Sensing Systems, Santa Rosa, CA. 2015. Available online: www.remss.com/measurements/ccmp (accessed on 30 March 2021).
50. Zuo, H.; Balmaseda, M.A.; Tietsche, S.; Mogenssen, K.; Mayer, M. The ECMWF Operational Ensemble Reanalysis–Analysis System for Ocean and Sea Ice: A Description of the System and Assessment. *Ocean Sci.* **2019**, *15*. [\[CrossRef\]](#)
51. Fetterer, F.; Knowles, K.; Meier, W.N.; Savoie, M.; Windnagel, A.K. Sea Ice Index, Version 3. Boulder, Colorado USA. NSIDC: National Snow and Ice Data Center. 2017. Available online: <https://doi.org/10.7265/N5K072F8> (accessed on 30 March 2021).
52. Peterson, B.J. Trajectory Shifts in the Arctic and Subarctic Freshwater Cycle. *Science* **2006**, *313*. [\[CrossRef\]](#)
53. Aune, M.; Aniceto, S.; Biuw, M.; Daase, M.; Falk-Petersen, S.; Leu, E.; Ottesen, C.; Sagerup, K.; Camus, L. Seasonal ecology in ice-covered Arctic seas—Considerations for spill response decision making. *Mar. Environ. Res.* **2018**, *141*. [\[CrossRef\]](#)
54. Nichols, R.E.; Subrahmanyam, B. Estimation of Surface Freshwater Fluxes in the Arctic Ocean Using Satellite-Derived Salinity. *Remote Sens. Earth Syst. Sci.* **2019**, *2*, 2. [\[CrossRef\]](#)
55. Mazloff, M.R.; Heimbach, P.; Wunsch, C. An Eddy-Permitting Southern Ocean State Estimate. *J. Phys. Oceanogr.* **2010**, *40*. [\[CrossRef\]](#)
56. Kawai, Y.; Osafune, S.; Masuda, S.; Komuro, Y. Relations between Salinity in the Northwestern Bering Sea, the Bering Strait Throughflow and Sea Surface Height in the Arctic Ocean. *J. Oceanogr.* **2018**, *74*. [\[CrossRef\]](#)
57. Olmedo, E.; Gabarró, C.; González-Gambau, V.; Martínez, J.; Ballabrera-Poy, J.; Turiel, A.; Portabella, M.; Fournier, S.; Lee, T. Seven Years of SMOS Sea Surface Salinity at High Latitudes: Variability in Arctic and Sub-Arctic Regions. *Remote Sens.* **2018**, *10*, 1772. [\[CrossRef\]](#)
58. Supply, A.; Boutin, J.; Vergely, J.L.; Kolodziejczyk, N.; Reverdin, G.; Reul, N.; Tarasenko, A. A new methodology to derive SMOS sea surface salinity in the Arctic Ocean. *Remote Sens. Environ.* **2020**, *249*, 249–112027. [\[CrossRef\]](#)
59. Houpert, L.; Inall, M.; Dumont, E.; Gary, S.; Johnson, C.; Porter, M.; Johns, W.; Cunningham, S. Structure and Transport of the North Atlantic Current in the Eastern Subpolar Gyre From Sustained Glider Observations. *J. Geophys. Res. Ocean.* **2018**, *123*. [\[CrossRef\]](#)
60. Carvalho, K.S.; Wang, S. Sea Surface Temperature Variability in the Arctic Ocean and Its Marginal Seas in a Changing Climate: Patterns and Mechanisms. *Glob. Planet. Chang.* **2020**, *193*. [\[CrossRef\]](#)
61. Jung, O.; Sung, M.-K.; Sato, K.; Lim, Y.-K.; Kim, S.-J.; Baek, E.-H.; Jeong, J.-H.; Kim, B.-M. How Does the SST Variability over the Western North Atlantic Ocean Control Arctic Warming over the Barents–Kara Seas? *Environ. Res. Lett.* **2017**, *12*. [\[CrossRef\]](#)
62. di Lorenzo, E.; Mantua, N. Multi-Year Persistence of the 2014/15 North Pacific Marine Heatwave. *Nat. Clim. Chang.* **2016**, *6*, 1042–1047. [\[CrossRef\]](#)
63. Hu, Z.Z.; Kumar, A.; Jha, B.; Zhu, J.; Huang, B. Persistence and Predictions of the Remarkable Warm Anomaly in the Northeastern Pacific Ocean during 2014–2016. *J. Clim.* **2017**, *30*, 689–702. [\[CrossRef\]](#)

-
64. Hartmann, D.L. Pacific Sea Surface Temperature and the Winter of 2014. *Geophys. Res. Lett.* **2015**, *42*. [[CrossRef](#)]
 65. Petty, A.A.; Stroeve, J.C.; Holland, P.R.; Boisvert, L.N.; Bliss, A.C.; Kimura, N.; Meier, W.N. The Arctic Sea Ice Cover of 2016: A Year of Record-Low Highs and Higher-Than-Expected Lows. *Cryosphere* **2018**, *12*, 433–452. [[CrossRef](#)]
 66. Tilling, R.L.; Ridout, A.; Shepherd, A.; Wingham, D.J. Increased Arctic Sea Ice Volume after Anomalously Low Melting in 2013. *Nat. Geosci.* **2015**, *8*. [[CrossRef](#)]
 67. Francis, J.A.; Chan, W.; Leathers, D.J.; Miller, J.R.; Veron, D.E. Winter Northern Hemisphere Weather Patterns Remember Summer Arctic Sea-Ice Extent. *Geophys. Res. Lett.* **2009**, *36*. [[CrossRef](#)]
 68. Vihma, T. Effects of Arctic Sea Ice Decline on Weather and Climate: A Review. *Surv. Geophys.* **2014**, *35*, 1175–1214. [[CrossRef](#)]
 69. Overland, J.E.; Wang, M. Recent Extreme Arctic Temperatures Are Due to a Split Polar Vortex. *J. Clim.* **2016**, *29*. [[CrossRef](#)]
 70. Wang, Q.; Marshall, J.; Scott, J.; Meneghello, G.; Danilov, S.; Jung, T. On the Feedback of Ice–Ocean Stress Coupling from Geostrophic Currents in an Anticyclonic Wind Regime over the Beaufort Gyre. *J. Phys. Oceanogr.* **2019**. [[CrossRef](#)]
 71. Dodd, P.A.; Heywood, K.J.; Meredith, M.P.; Naveira-Garabato, A.C.; Marca, A.D.; Falkner, K.K. Sources and Fate of Freshwater Exported in the East Greenland Current. *Geophys. Res. Lett.* **2009**, *36*. [[CrossRef](#)]
 72. Jahn, A.; Aksenov, Y.; de Cuevas, B.A.; de Steur, L.; Häkkinen, S.; Hansen, E.; Herbaut, C.; Houssais, M.N.; Karcher, M.; Kauker, F.; et al. Arctic Ocean Freshwater: How Robust Are Model Simulations? *J. Geophys. Res. Ocean.* **2012**, *117*. [[CrossRef](#)]
 73. de Steur, L.; Peralta-Ferriz, C.; Pavlova, O. Freshwater Export in the East Greenland Current Freshens the North Atlantic. *Geophys. Res. Lett.* **2018**, *45*, 13359–13366. [[CrossRef](#)]
 74. Skliris, N.; Marsh, R.; Mecking, J.V.; Zika, J.D. Changing Water Cycle and Freshwater Transports in the Atlantic Ocean in Observations and CMIP5 Models. *Clim. Dyn.* **2020**, *54*, 4971–4989. [[CrossRef](#)]
 75. de Steur, L.; Pickart, R.S.; Macrandar, A.; Våge, K.; Harden, B.; Jónsson, S.; Østerhus, S.; Valdimarsson, H. Liquid Freshwater Transport Estimates from the East Greenland Current Based on Continuous Measurements North of Denmark Strait. *J. Geophys. Res. Ocean.* **2017**, *122*. [[CrossRef](#)]
 76. Nghiem, S.V.; Hall, D.K.; Mote, T.L.; Tedesco, M.; Albert, M.R.; Keegan, K.; Shuman, C.A.; DiGirolamo, N.E.; Neumann, G. The Extreme Melt across the Greenland Ice Sheet in 2012. *Geophys. Res. Lett.* **2012**, *39*. [[CrossRef](#)]
 77. Bamber, J.; van den Broeke, M.; Ettema, J.; Lenaerts, J.; Rignot, E. Recent Large Increases in Freshwater Fluxes from Greenland into the North Atlantic. *Geophys. Res. Lett.* **2012**, *39*. [[CrossRef](#)]
 78. Josey, S.A.; Marsh, R. Surface Freshwater Flux Variability and Recent Freshening of the North Atlantic in the Eastern Subpolar Gyre. *J. Geophys. Res. Ocean.* **2005**, *110*, 1–17. [[CrossRef](#)]